

REFERENCE : AE12

**TITLE : PERFORMANCE PREDICTION AND FLOWFIELD ANALYSIS OF ROTORS IN HOVER, USING A COUPLED EULER/BOUNDARY LAYER METHOD**

AUTHORS :

P. BEAUMIER / ONERA - Châtillon  
C. CASTELLIN / EUROCOPTER - Marignane  
G. ARNAUD / EUROCOPTER - Marignane

The performance prediction of helicopter in hover is of key importance for manufacturers because hover is a design configuration for the definition of a rotorcraft. A lot of efforts have been made for more than 10 years all over the world in order to develop and validate numerical methods based on CFD. An Euler method (WAVES) developed by ONERA and coupled with a boundary layer code (MI3DI) is presented, validated and applied to compute the total performance of rotors with different tip shapes. A new boundary condition for the Euler code has been tested and enables better calculation by eliminating "numerical" recirculation. The code has demonstrated its ability to rank two rotors with different planforms in good agreement with experiment. Under industrial requirements new grid strategies have been studied and should allow to reduce CPU time consumption. It is shown that WAVES/MI3DI can be efficiently used in the aerodynamic design process of a new rotor.

**NOTATIONS**

R	rotor radius
$\Omega$	rotational angular velocity
a <sub>∞</sub>	speed of sound
$M_{QR} = \Omega R / a_{\infty}$	tip rotational Mach number
$M = r/R M_{QR}$	blade sectional Mach number
$\rho_{\infty}$	fluid density
b	number of blades
c	blade reference chord
$S = \pi R^2$	rotor disk surface
$\sigma = bRc/S$	solidity
$F_z$	rotor thrust
$Z_b = 100F_z / (1/2\rho_{\infty} S (\Omega R)^2)$	rotor thrust coefficient
P	power consumed by the rotor
$FM = F_z^{3/2} / (P(2\rho_{\infty} S)^{1/2})$	figure of merit
$C_z$	2D lift coefficient (rotor axis)
$C_x$	2D drag coefficient (rotor axis)
$C_x M^3$	2D local power coefficient (rotor axis)
$\theta_0$	collective pitch angle
$\rho$	local fluid density
(u,v,w)	absolute fluid velocity
e	internal fluid energy
$E = e + 1/2V^2$	total fluid energy

**INTRODUCTION**

The hover configuration is a sizing case for helicopter design. So it is of great interest for industry to predict this performance for a given aircraft but also to be able to compare two rotors. Although the hover case seems easy because of the steadiness in the rotating frame, the problem is very difficult due to vortex generation at blade tip and interaction with the next blade. The first consequence is an increase of iterations required to converge (compared with isolated blade or forward flight) and the second one is the difficulty to compute an accurate performance prediction due to vortical effects. The use of simplified methods, like the lifting line theory even with a free wake model, is limited for complex blade tips because of the non trivial links between geometrical parameters and vortex characteristics. The use of 3D vortex capturing methods are therefore required. For more than 10 years, a lot of studies have been carried out on numerical calculation resolving fluid mechanic equations. Several codes were developed from potential methods with vorticity velocity (to avoid vorticity diffusion encountered with Euler methods), like PHOENIX code [1], to Euler and Navier-Stokes methods, like TURNS code [2], which in the last case could handle more correctly the tip vortex

generation and the unattached flow in the inner part of the blades.

An EULER method for the prediction of rotor aerodynamics in hover, WAVES, was developed by ONERA under the following EUROCOPTER industrial requirements : be capable to compute hover performance, including power, be a robust and easy to use tool for intensive use, be as low as possible computational time demanding to allow everyday industrial applications and rotor optimization.

To fulfill these requirements, an original implicit explicit algorithm was selected, which limits numerical dissipation. This EULER code was coupled to a 3D integral boundary layer method in order to compute the different terms (viscous, inviscid) of the power consumed by the rotor. A description of the method is given in a first part with a study of two types of boundary conditions. In a second part, convergence criteria and grid convergence problems are addressed for quality of the solution assessment. Due to industrial requirements on calculation time, an attempt to optimize a grid is also proposed in order to reduce numerical diffusion with a given number of grid points. In the last part, the comparison of the performance of two rotors with different tip shapes is presented.

## 1. COMPUTATIONAL METHOD

### 1.1 Euler solver WAVES

The solver presented and used in the present paper was originally developed at ONERA by Sidès and Boniface [3,4]. One particularity of the method is that it works with a centered scheme without explicit artificial viscosity in transonic regime. The Euler equations are formulated in the rotating frame using as unknowns the five components vector ( $\rho, \rho u, \rho v, \rho w, pE$ ) of the absolute flow values expressed in the rotating frame. A periodicity condition in the upstream and downstream planes accounts for the influence of the other blades. This condition avoids any extrapolation of the solution due to the coincidence of the grid nodes in the upstream and downstream planes. For steady flows (such as hover in the rotating frame) a local time step is used in order to accelerate convergence. The boundary conditions (fig. 1) used in the original code are:

- a slip boundary condition on the airfoil surface (no viscous effect)
- a periodicity condition ensured by the use of coincident upstream and downstream surfaces in order to simulate the multibladed rotor
- boundary conditions based on characteristic theory for all other boundaries (upper, lower, inner and outer surfaces). At each grid point of these surfaces, depending on whether the fluid is locally subsonic or supersonic and depending on whether the fluid enters the computational domain or not, the conservative variables at this grid point are computed from the conservative variables inside the computational domain and their values assumed outside of it. It was initially assumed that the fluid had zero velocity outside the computational domain.

### 1.2 Boundary layer code MI3DI

One method to account for viscous effects in an Euler solver is to couple it with a boundary layer code. To achieve this, the MI3DI boundary layer method was developed at ONERA/CERT with specific adaptations for rotor applications [5]. This method solves for the laminar and turbulent 3D compressible boundary layer integral equations. In particular, the transition between laminar and turbulent flows is accounted for according to several transition criteria (longitudinal or transversal instability, ...). More detailed informations about this method can be found in [5]. The method only requires the knowledge of the 3D coordinates of the blade upper and lower surfaces, the density and relative velocities at each grid point of these surfaces. In the present application, these quantities are provided by the Euler code WAVES. Note that such a boundary layer code can only calculate attached flows.

### 1.3 Coupling procedure WAVES/MI3DI

In order to account for the modification of pressure distribution generated by the boundary layer, a special boundary condition was implemented in the Euler solver. A non zero velocity normal to the airfoil accounts for the thickening of the airfoil due to the boundary layer. An equivalent "transpiration" angle is calculated from the spatial derivatives (in the chordwise and spanwise directions) of the boundary layer thicknesses  $\Delta 1$  and  $\Delta 2$  [5]. Note that this method may not be adequate when the turbulent boundary calculation is stopped because of numerical instabilities or physical unattached flows. In this

case, an extrapolation of the transpiration angle is done between the last calculated point in the chordwise direction and the trailing edge.

#### 1.4 Adequate boundary conditions for hover

One of the major difficulties when computing hover conditions with CFD methods is the choice of appropriate boundary conditions on external surfaces. The use of the "standard" boundary conditions presented above (assuming 0 velocity outside the computational domain) leads to a solution (represented in fig. 2a) that is not representative of hover, with a large recirculating flow inside the computational domain and almost no fluid entering the domain by the upper surface. It is believed that the external grid boundaries used for the present applications are too close to the rotor (2 rotor radii for the present calculation) to assume that the fluid outside the computational domain has 0 velocity. This problem was initially addressed by Srinivasan [6] who developed some specific boundary conditions based on momentum theory. These boundary conditions have been extensively used since that time [2,7]. In a way similar but not equivalent to what is done in [6], the boundary conditions used in the Euler code WAVES on the external (upper, lower and outer) boundaries have been modified by simply assuming that the fluid outside these boundaries has a non zero velocity  $V^*$  which can be evaluated thanks to momentum theory by:

$$V^* = - S/4\pi r^2 (Fz/2\rho_\infty S)^{1/2} e_r \text{ (Eq. 1)}$$

where  $r$  is the distance between the point on the grid surface and the center of rotor disk of the reference frame and  $e_r$  is the radial unit vector. Note that  $V^*$  depends on the rotor thrust  $Fz$ , which is an unknown of the problem. In the method developed for the present study,  $Fz$  is calculated at each iteration  $n$  by pressure integration (when no boundary layer is used) on the airfoil and used at iteration  $n+1$  to calculate  $V^*$  so that the procedure is self-consistent (no need of the experimental rotor thrust).

Thanks to this so-called "Froude boundary conditions", the flowfield in a vertical plane located 10 degrees behind the blade seems to be a good qualitative representation of that of a rotor in hover (fig. 2b).

## 2. INITIAL VALIDATION

### 2.1 Boundary layer transition

The first validation proposed in this part is to check that the coupled WAVES/MI3DI method is able to predict accurately the state of the boundary layer (laminar, turbulent) or at least the chordwise location of the transition between laminar and turbulent flow.

To achieve this, in-flight blade surface measurements were performed on a Dauphin aircraft for conditions as close as possible to hover. Before the flight, the blades were painted with acenaphtene painting; during the hover flight, the transition between laminar and turbulent boundary layer led to a sublimation of the painting; after the flight, photos of the blade were taken in order to determine the location of the transition. Depending on the natural unsteadiness of the flow during the flight, on the duration of the test, on the quality (uniformity) of the painting, the results of such tests exhibit some scatter. Therefore, different flights corresponding to the same test condition are used in this part: their analysis shows that the chordwise position of the transition is measured within a range of +/- 7% blade chord scattering, which is believed to be a reasonable accuracy.

The measured data used to simulate numerically these tests with the WAVES/MI3DI code are the following:  $M_{OR}=0.643$ ,  $\theta_0=6.61^\circ$ .

After convergence, the CFD method calculates a thrust coefficient  $Zb=13.6$ , whereas the measured  $Zb$  was equal to 13.4, which is a surprisingly very good result, considering the uncertainty due to the tests unsteadiness and the measured value of collective pitch  $\theta_0$ . Fig. 3 compares the calculated state of the boundary layer (grey scale) with the measured position of the transition. The agreement is almost perfect on the upper surface and is reasonably good on the lower surface, except near the blade tip. In particular, the presence of a large laminar area on the lower surface is well predicted by the calculation. Note the presence of non calculated (unattached?) flows in the inner part of the upper surface of the blade.

This overall good agreement between calculation and experiment validates the boundary layer transition prediction.

## 2.2 Code response to an increase in blade geometric twist.

It is well known that the best way to increase the hover performance of rotors is to increase their geometric twist. No experimental database with rotors differing only by their geometric twist was available to the authors of the present paper. Therefore, only a numerical parametric study is proposed in this part.

The reference rotor for this study is the 4 bladed 7A rotor equipped with rectangular blades (Tab. 1). While conserving the same blade geometry as for the 7A blades, two other "hypothetical" blades were defined by increasing the linear twist: the so-called 7B blade with  $-12^\circ / R$  twist and the 7C blade with  $-16^\circ / R$  twist.

Rotor radius	R=2.1m
Blade chord	c=0.14m
Airfoils	OA213 (13% thickness) from root to 0.75R OA209 (9% thickness) from 0.9R to tip
Linear aerodynamic twist	$-8.3^\circ / R$

Tab. 1 : Main characteristics of the 7A rotor.

Grids including approximately 250000 points were generated for each of these rotors and a sweep in collective pitch angles was performed. After convergence, Fig. 4a clearly shows the increase of FM from the 7A to the 7B blades and from the 7B to the 7C blades: the difference in FM between the 7A and the 7C blades reaches 3.5 counts of FM (one count corresponding to  $\Delta FM = 0.01$ ). This increase in performance is attributed to a change in spanwise loads distributions with lower  $C_z$  values near the blade tip for the highly twisted blades (7B and 7C) than for the 7A blade, thus leading to less intense circulation (fig. 4b). This circulation reduction also decreases the local power consumed by the sections located near the blade tip: this is illustrated by figure 4c representing the  $C_x M^3$  drag coefficients (which represents a nondimensionnal 2D power coefficient).

It is concluded that the present computational method WAVES/MI3DI succeeds in qualitatively predicting the increase of FM due to an increase in blade geometric twist.

## 3. MESH INFLUENCE AND CONVERGENCE

After these and other tests on basic rotors, it was decided to install the code in the industrial computational environment at EUROCOPTER. To go on validation, a worksharing between the industry and the research center was set up, and the 7A/7AD Modane rotors were selected for their close geometry to production rotors. For this validation phase, the industrial practical issues were emphasized.

### 3.1 convergence criteria

For example, it is of prime importance to define robust criteria of convergence before to address the problem of grid refinement effect on the result and to judge the quality of a numerical solution. Residuals on density  $\rho$  and some global performance terms (of industrial interest) as a function of the number of iterations are plotted for 4 grids on figures 5.

Fig. 5a shows that the residuals on density  $\rho$  are reduced by 3 orders of magnitude for the coarse grid but only 2 orders of magnitude for the very fine grid. All these curves have reached their final values after around 5 000 iterations. Besides, the history of figure of merit (fig. 5b) and thrust (fig. 5c) shows that 5 000 to 10 000 iterations more are needed to converge on performance. Moreover, the Figure of Merite and thrust histories can provide usefull guidings to evaluate time/accuracy compromise. An acceptable accuracy for rotor optimization in hover has to be lower than  $\pm 1.5$  point of figure of merit if we want to be able to rank two rotors. This value can be compared with the experimental scattering on figure of merit measurement or with its consequence on helicopter performance : 3 more points on FM means one extra pax on a Dauphin. Another interest of these curves is to underline the unsteadiness of the solution for higher thrust and to give the amplitudes of thrust and power variations. Residuals,  $K_p$  distribution, or circulation histories are not so selective : they are not sensitive enough as far as power performance is concerned. But the residuals keep their interest to verify the quality of the convergence.

Therefore, the best way to know if the solution is converged or not is to follow the history of FM and thrust. For the coarse, medium and fine grids, a very good convergence is achieved after 15000 iterations. For the very fine grid, more iterations would be required. It is of importance to point out here that

the different grids converge on different results. Convergence does not mean that the right solution is obtained. This is the topic of the following paragraph.

### 3.2 Grid convergence study

Before comparing the calculated figure of merit or thrust with any experimental data, it is important to quantify how much the computed solution is grid dependent. This is particularly relevant for Euler (or Navier-Stokes) solvers because numerical dissipation, which is typically grid dependent, is an obstacle to a good description of vortex convection. The mesh generator used here is an internal single block structured mesh generator with a C-H topology. In this part, a basic "coarse" grid is generated for the 7A rotor described above with a collective pitch angle  $\theta_0=5.97^\circ$ . This grid contains approximately 250000 points distributed according to Tab. 2. From the coarse grid, the number of points in each direction (I, J or K) is multiplied by a factor that is progressively increased: three new grids respectively called "medium", "fine" and "very fine" grids are thus created (Tab. 2), with the same mesh technique.

Number of points (I)	(J)	(K)	Total	
coarse grid	181	38	38	250000
medium grid	221	46	46	450000
fine grid	255	52	52	700000
very fine grid	285	59	59	1000000

Tab. 2 : Main characteristic of the four grids for the 7A rotor in chordwise (I), spanwise (J) and normal(K) direction.

It is very satisfying to see that the difference in FM between the converged results with the fine and very fine grids is very small (less than 1 count of FM), whereas it is much higher (5 counts) between the coarse and very fine grids (fig. 6a and 6b). This is confirmed by figure 7 which shows the vorticity contour levels in a vertical plane located  $10^\circ$  after of the blade: this figure shows that the vortex is better captured with the very fine grid than with the coarse grid, which is what was expected. But it can also be seen in figure 8 that the location of vortex just before it interacts the blade ( $10^\circ$  ahead of the blade) moves inboard when the grid density is increased, probably because of an increased wake contraction: however, the center of the vortex with the fine and very fine grids are actually very close which strengthens the conclusion that the solution

obtained with the very fine grid (with 1000000 points) is almost grid converged.

In order to validate calculations, an experiment performed in Eurocopter outdoor facility is used. Such tests were done for the 7A rotor and it is assumed that the flowfield around the rotor is of good quality (rotor positionned upside down to ensure to be out of ground effect, limited unsteadiness). Only global performance (thrust, power and figure of merit) are available for these tests. Both calculations with 250000 and 1000000 points follow reasonably well the experiment but it is clear that the calculation with the very fine grid is in better agreement with the measured data than the calculation with the coarse grid, in terms of thrust for a given collective pitch angle (fig. 9a) and in terms of figure of merit (fig. 9b). However, there is still an overestimate of figure of merit by 3 counts, even with the very fine grid. This overestimate is certainly due to a lack of accuracy in capturing the vortical effects because of numerical dissipation. As said before, there were no surface pressure and no vortex trajectories measurements during these tests, so that it is very difficult to analyze in details the reasons of the discrepancies between calculations and experiment.

Very fine grids with at least 1000000 points seem to provide a solution in good agreement with experiment. However, such calculations are very much time consuming because of the grid density and of the number of iterations to be performed in order to reach a converged solution. As an example, 25 hours are required on a Dec Alpha to converge with a coarse grid whereas more than 120 hours are needed with a very fine grid just for one trim. Such computations are not realistic for industrial applications. Consequently, in order to reduce the CPU time and simultaneously try not to deteriorate too much the quality of the solution, new grid strategies have been studied at Eurocopter and are presented in the next section.

### 3.3 New grid strategy

Grid generation for rotors in hover is very difficult due to the different scales of aerodynamic phenomena. The general flow (contracting flow) is one rotor radius scaled, the flow around blade sections is one chord scaled and the vortex is one blade thickness scaled. For the 7AD rotor which differs from the 7A by a swept and anhedral tip (fig.16), the ratios between these scales are respectively 1, 1/30 and 1/450. The difficulty is here

increased by the use of single block C-H structured grids and periodicity condition.

The previous calculations have emphasized the importance of vortex diffusion. In order to get some understanding about this diffusion, the evolution of the maximum of vorticity is plotted in fig.10a in function of the tip vortex age, in logarithmic scale. Two slopes in fig10a are clearly seen and the dissipation is reduced after the periodicity plane. The difference in slope could be attributed to the cell size variation along tip vortex path in I and K direction (fig. 10b). The cell size is small near the blade and increases towards the periodicity plane (in these directions) and vice versa. So, when the cell size is increasing the vortex diffusion is large, while it is smaller when the cell size is decreasing. An idea to optimize the grid is thus to keep size in K direction constant along vortex path, which is easy to perform with this mesh by contracting and stretching the grid around the guessed vortical area. Two grids have been made (with 360000 points). The former is classical while the latter is optimized (fig. 11) as explained before. From 1 000 000 points to 360 000 points as much as 60 % CPU time can be saved. Looking at the spanwise vertical velocities two chords behind the blade, we can see that an identical vortex has been emitted at the blade tip (fig. 12) for the two meshes (same grid on the blade). However, the spanwise vertical velocities two chords ahead of the blade (which can be correlated to the induced velocities on the blade sections) are different at tip vortex location (fig. 12). The peak velocity induced by this vortex is increased by 25% for the optimized grid. The effect on vorticity diffusion can be seen on vorticity contour levels on the periodicity plane (fig. 11). The performance calculated by the code is modified by this more concentrated vortex. On figure 13, the calculated spanwise  $C_z M^2$  clearly shows the influence of grid modification on local thrust. As demonstrated, the only difference is due to diffusion along vortex path.

Another study on grid size has demonstrated the relationship between the spanwise cell size at blade tip and the maximum vorticity emitted. However, the C-H topology doesn't allow to have a "flat vertical" blade tip (but only "triangular" to limit grid deformation). Therefore, to avoid any differences due to grid between calculations on two rotors, it is recommended to size the last spanwise cell at the blade tip as a function of blade tip thickness. This might however not be enough, since in this outer region the vortex roll-up is a viscous

process, which cannot be accounted for by an Euler method.

With such "rules of art" it is thus possible to create similar and accurate grids on two different rotors, while saving computational time.

#### 4. APPLICATION: COMPARISON OF 7A AND 7AD ROTORS

The final goal of the computation is not only to be able to obtain good comparisons between calculations and experiment but mostly to predict and understand the difference in figure of merit between two rotors. Consequently, calculations have been performed on the 7A rotor (equipped with rectangular blades) and the 7AD rotor equipped with parabolic swept tip. The two rotors have exactly the same characteristics (same twist, same airfoils) and only differ by their shapes from 0.95 to 1R. They were both tested in the same conditions at the EUROCOPTER outdoor facility.

The calculations for these two rotors use very similar grids (in terms of number of points, nodes distributions and grid extension): these grids were defined according to the considerations mentioned in the previous section. Three conditions were calculated for the following collective pitch angles:  $\theta_0=5.97^\circ$ ,  $7.51^\circ$  and  $8.29^\circ$ . The differences in figure of merit between the 7A and the 7AD rotors are represented in figure 14. Both experiments and calculations show that the 7AD rotor has a higher FM than the 7A rotor, in particular for the highest collective pitch angles (3 counts of FM). This difference does not really come from differences in thrust levels, which are similar for the two rotors, but rather comes from consumed power. Indeed, the calculated spanwise  $C_x M^3$  coefficients (fig. 15a) clearly shows a decrease of power consumption in the tip portion of the 7AD blade, due to the swept parabolic tip shape. This power decrease is accompanied by a reduction of the strength of the vortices emitted by the 7AD blade (fig. 15b): in addition, the vortices of the 7AD rotor are emitted a little bit more inboard than the vortices emitted by the 7A rotor. Finally, figure 16 shows the qualitative differences in the vortex emission between the two blades: here again, it seems that the vortical structures for the 7AD blade are a little bit weaker in intensity than those of the 7A blade.

This shows that the Euler / Boundary layer code WAVES/MI3DI succeeds in predicting the

differences in figure of merit between the 7A and 7AD rotors which only differ by their blade tip shapes. In addition, it provides some understanding of the reasons of such differences on total performance, thanks to an analysis of the vortical structures and blade surface loading.

## CONCLUSIONS

The Euler method WAVES developed by ONERA meets most of the Eurocopter industrial requirements. Performance is computed with less than 3 points difference with measurements. Computational time for a whole polar curve is of the order of a week in the industrial environment, which is considered acceptable. Robustness of the method has been demonstrated in the range of the sea level rotor definition point. This statement has been achieved thanks to a rigorous methodology of industrialisation.

After former usual checkings, a close collaboration has been set up between ONERA and EUROCOPTER to validate the code under industrial environment. During this necessary phase, such problems as mesh generation techniques but also convergence criteria were addressed, which led to define "instructions for industrial use" for this code. The code ability to distinguish two rotors, as far as their performance is concerned, was demonstrated.

In the future, some efforts will be made in order to try to reduce the numerical diffusion of vorticity, for example by testing some Euler-Lagrange coupling methods; such methods, already operational for fixed wing applications have to be extended to the particular case of rotating blades. In addition, the validation of Navier-Stokes solvers, instead of Euler/Boundary Layer methods, for the rotor in hover is under way. It is believed that solving the Navier-Stokes equations, with appropriate turbulence models, will help to calculate the rotor figure of merit for conditions close to stall, which is presently not possible with the current WAVES/MI3DI code. Finally, the forward flight version of the Euler code WAVES is presently being validated. All these CFD codes, developed at ONERA, will have to be transferred to industry, following the same methodology as the one presented in this study, which proved its efficiency.

## ACKNOWLEDGEMENTS

The authors would thank the French Government Agency SPAé for their financial support in this research program.

## REFERENCES

- [1] Steinhoff J., Ramachandran K., Free wake analysis of compressible rotor flow in hover, 12th European Rotorcraft Forum, September 1986.
- [2] Wake B.E., Baeder J.D., Evaluation of the TURNS analysis for hover performance prediction, AHS Aeromechanics Specialists Conference, San Francisco, January 1994
- [3] Boniface J-C., Calcul d'écoulements compressibles autour de rotors d'hélicoptères en vol stationnaire ou en vol d'avancement par résolution des équations d'Euler, thèse de l'ENSAM, december 1995
- [4] Boniface J-C., Sides J., Numerical simulation of steady and unsteady flows around multibladed helicopter rotors in hover, 19th European Rotorcraft Forum, Cernobbio, September 14-16, 1993
- [5] Beaumier P., Houdeville R., 3D laminar-turbulent boundary layer calculations on helicopter rotors in forward flight: application to drag prediction, 21st European Rotorcraft Forum, Saint-Petersburg, August 30th - September 1st, 1995
- [6] Srinivasan G.R., Raghavan V., Duque, E.P.N., Flowfield analysis of modern helicopter rotor in hover by Navier-Stokes method, International Technical Specialists Meeting on Rotorcraft Acoustics and Rotor Fluid Dynamics, Philadelphia, 1991
- [7] Lemnios A. et al, Effect of tip vortex resolution on UH-60A rotor-blade hover performance calculations, 54th Annual Forum of the AHS, May 20-22, 1998

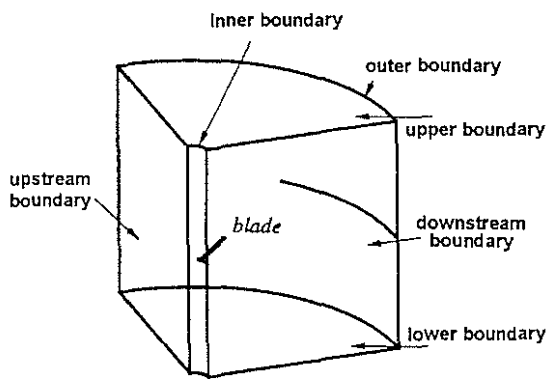


Figure 1 : Grid boundaries for the Euler solver.

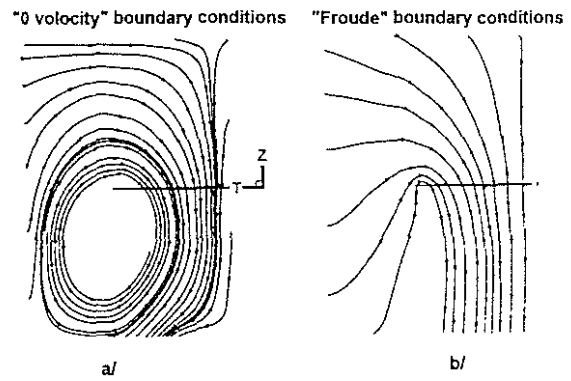


Figure 2 : Streamlines in a vertical plane located 10 degrees behind the blade of a hovering rotor.

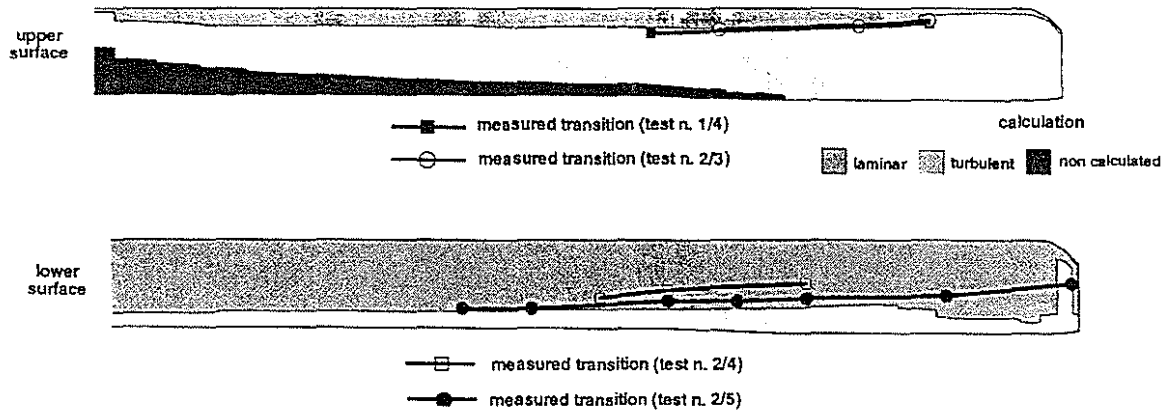


Figure 3 : Calculated state of boundary layer (grey scale) and measured transition position.

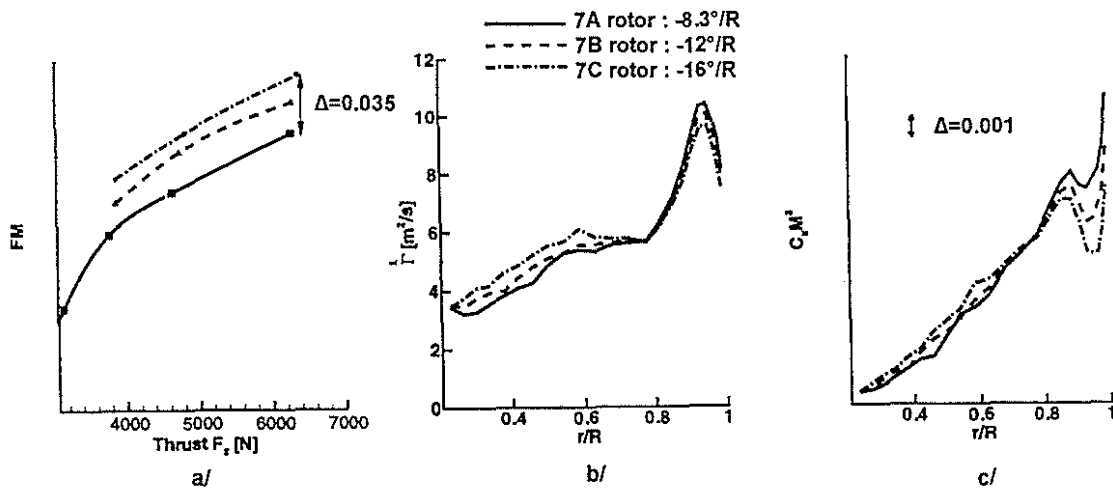


Figure 4 : Influence of blade twist on performance (a), circulation distribution (b) and power distribution (c).

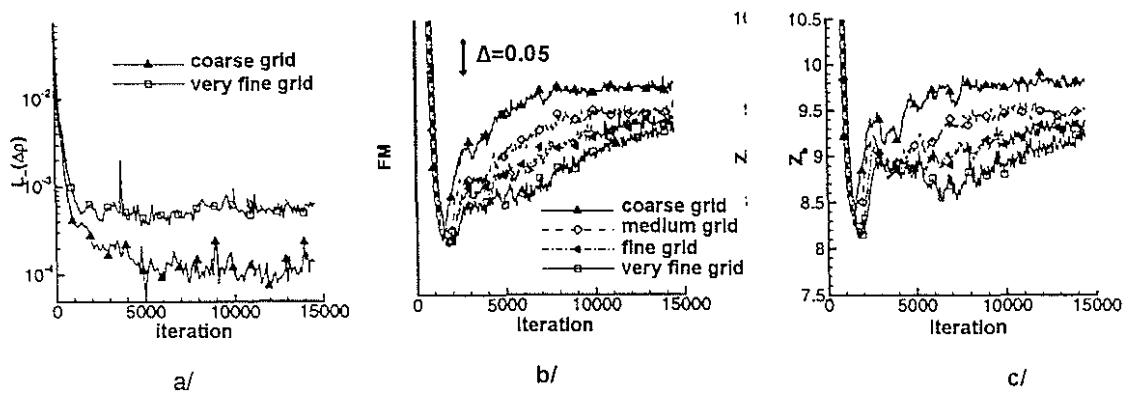


Figure 5 : Evolution of residuals on density (a), figure of merit (b) and thrust (c) as a function of iterations.

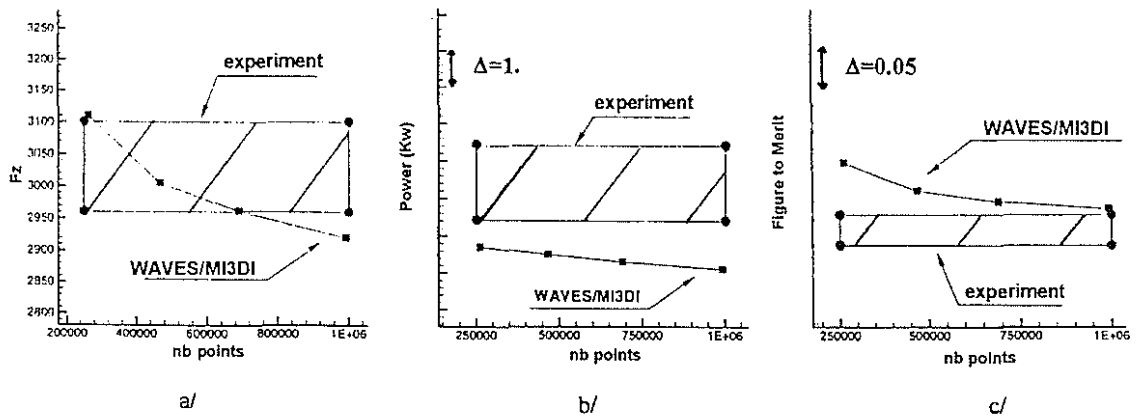


Figure 6 : Evolution of thrust (a), power (b) and figure of merit (c) as a function of number of grid points.

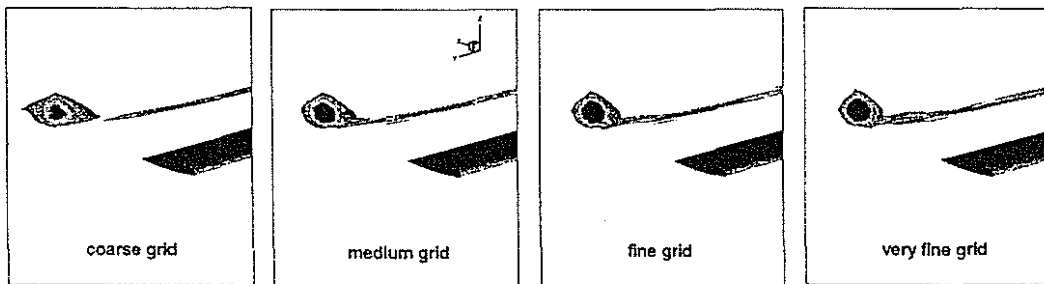


Figure 7 : Iso-vorticity contour line 0.1 in a vertical plane  $10^\circ$  after of the blade.

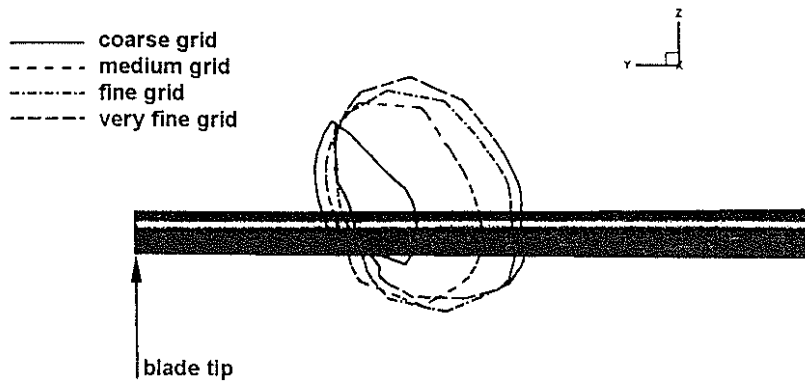


Figure 8 : Vortex position in a vertical plane 10° ahead of the blade.

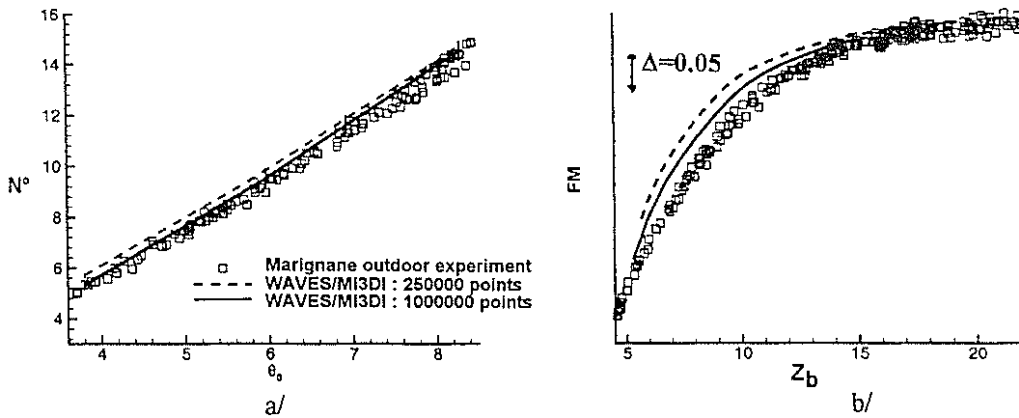


Figure 9 : Comparison of calculated and measured thrust and figure of merit for the 7A rotor.

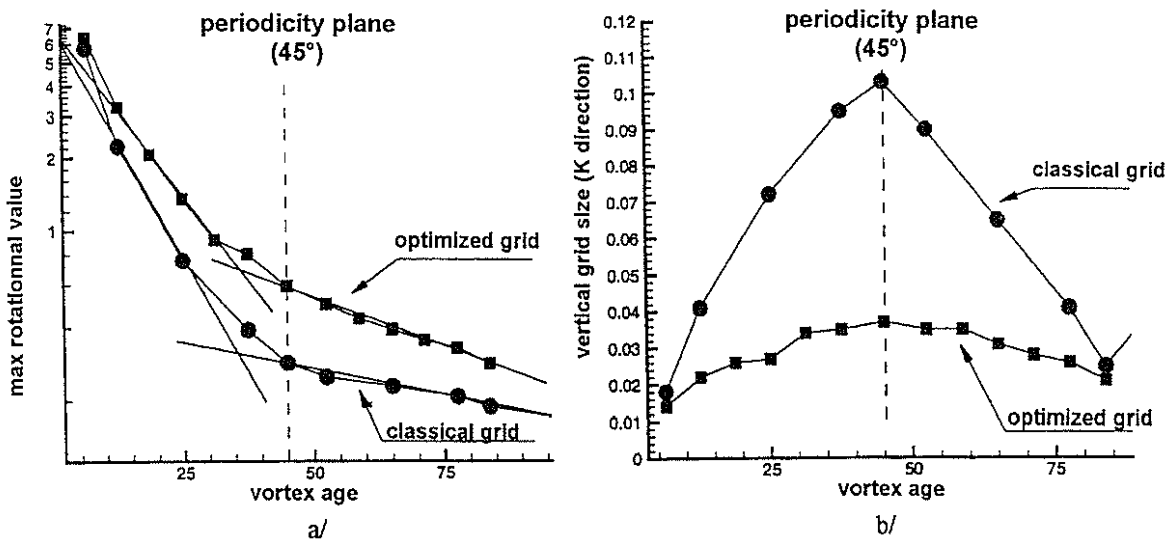
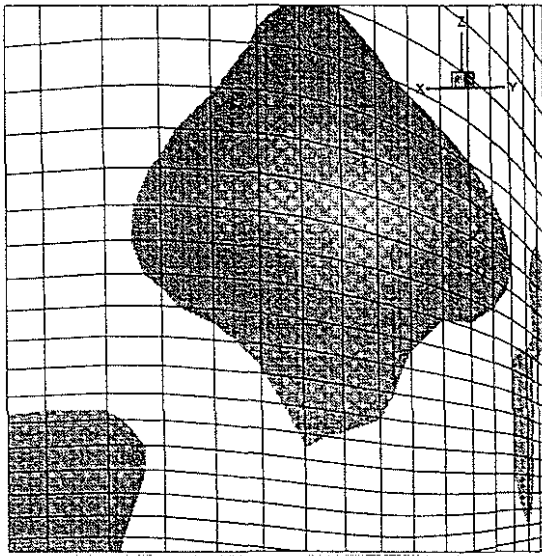
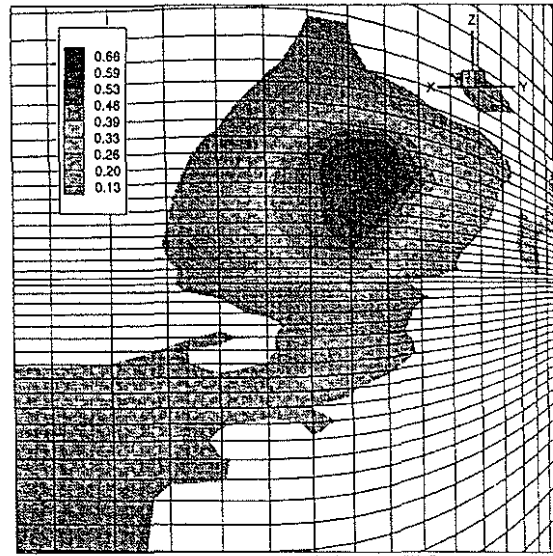


Figure 10 : Evolution along vortex path of maximum vorticity (a) and grid size in K direction (vertical) (b).



a/



b/

Figure 11 : Vorticity contour levels on the periodicity plane ( $45^\circ$ ) for classical grid (a) and optimized grid (b).

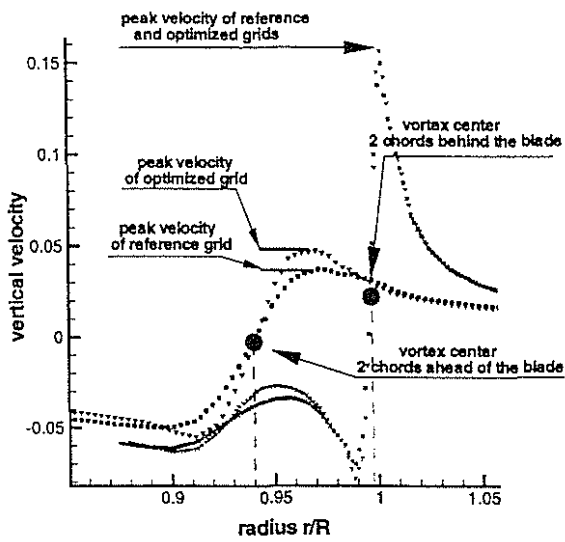


Figure 12 : Comparison of spanwise vertical velocity 2 chords ahead and behind blade

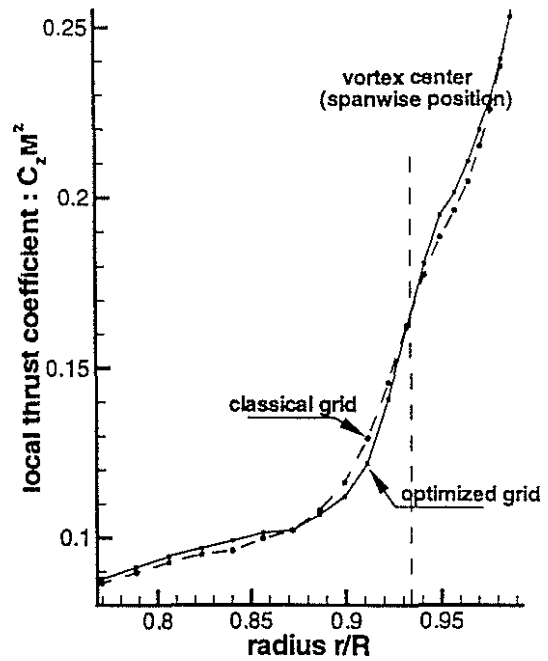


Figure 13 : Comparison of spanwise local thrust coefficient  $C_z M^2$

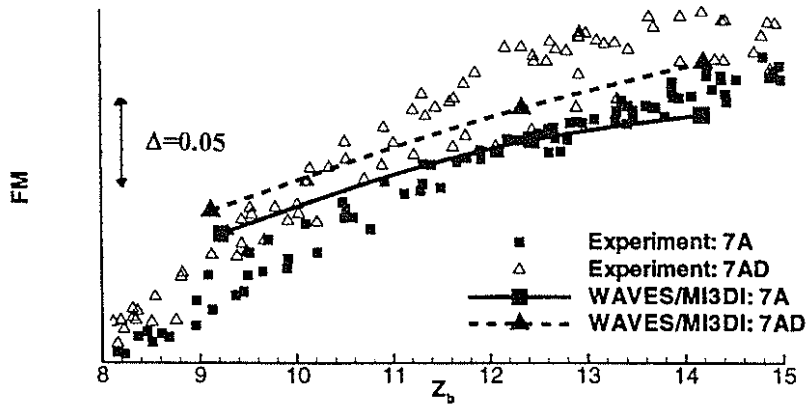


Figure 14 : Differences between the 7A and 7AD rotor in total performance.

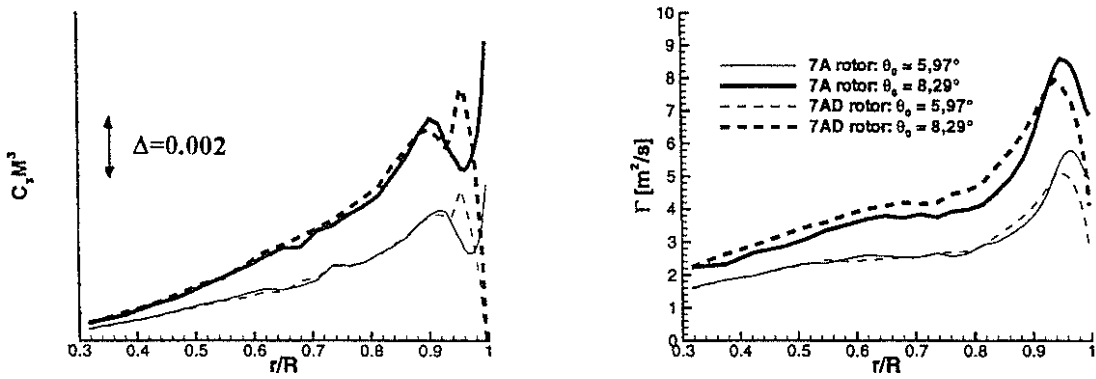


Figure 15 : Differences between the 7A and 7AD rotor in  $C_x M^3$  and circulation distributions

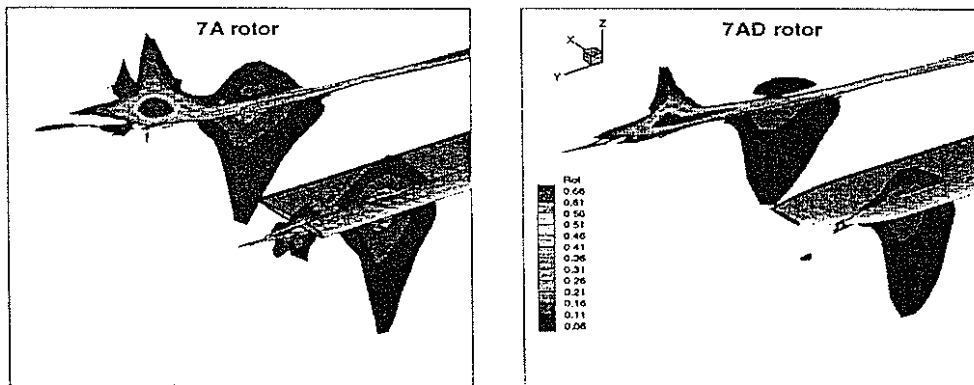


Figure 16 : Differences between the 7A and 7AD in vortex emission